J. Phys. IV France **138** (2006) 55–62
© EDP Sciences, Les Ulis
DOI: 10.1051/jp4:2006138007

X-ray generation by laser-cluster interaction

C. Deiss[1], N. Rohringer[1], J. Burgdörfer[1], E. Lamour[2], C. Prigent[2], J.P. Rozet[2] and D. Vernhet[2]

[1] *Institute for Theoretical Physics, Vienna University of Technology, 1040 Vienna, Austria*
[2] *INSP, Universités P. et M. Curie et D. Diderot, 140 rue de Lourmel, 75015 Paris, France*

Abstract. We investigate the efficient heating of quasi-free electrons during the interaction of short infrared laser pulses with large rare-gas clusters. In the framework of our mean-field classical transport simulation we are able to explain the emission of characteristic x-rays at moderate laser intensities ($I \sim 10^{15}\,Wcm^{-2}$) where the ponderomotive energy of the electrons is by far to low to allow for the creation of inner-shell vacancies. We identify large-angle elastic electron-ion scattering as an important heating mechanism at moderate laser intensities.

1. INTRODUCTION

The study of the interaction of intense short and ultra-short laser pulses with clusters has received much attention in the last decade [1]. When it comes to the emission of keV x-ray photons, rare-gas clusters unite the advantages of solid and gaseous targets: like solids they can provide large yields, yet they are relatively debris-free, just like gas targets.

In a simple picture, the dynamics during the laser-cluster interaction can be summarized as follows: the atoms of the cluster are first ionized by the incident laser pulse and electrons are set free in the cluster (inner ionization). The quasi-free electrons propagate in both the laser field and the field from the surrounding particles. Electron-impact ionization of cluster ions produces more quasi-free electrons, and inner-shell vacancies which are at the origin of x-ray radiation. As a fraction of the electrons leave the cluster (outer ionization), a net positive charge is left behind and the cluster begins to expand before disintegrating completely.

The spectroscopy of the emitted ions gives information on the system a few microseconds after the femtosecond laser-pulse and the cluster disintegration. The x-ray spectroscopy on the other hand allows measurements on a much shorter time-scale, down to few femtoseconds. The inner-shell vacancies in argon responsible for the 3.1 keV characteristic x-ray radiation can not be explained by field ionization for laser pulses with a peak intensity $I = 10^{21}\,Wcm^{-2}$. Consequently, the origin of these vacancies must be impact ionization by energetic electrons. The x-ray emission thus probes the high energy tail of the electron energy distribution, thereby providing valuable insight into the electronic dynamics which are the key to a detailed theoretical understanding of laser-cluster interaction. Furthermore, high-resolution x-ray spectroscopy determines the charge-state distribution of ions emitting the x-ray radiation.

Recent experiments [2, 3] found an unexpectedly low laser intensity threshold for x-ray production. When irradiating large clusters with $N > 10000$ argon atoms with infrared ($\lambda = 800\,nm$) laser pulses of duration $\tau = 60\,fs$ at FWHM, characteristic x-ray radiation could be measured for laser peak intensities as low as $I_{th} \approx 2.2.10^{15}\,Wcm^{-2}$. At this intensity, the ponderomotive energy $U_P = F^2/(4\omega^2)$ (atomic units are used unless otherwise stated) associated with the oscillatory motion of a free electron in a laser field with field strength F and frequency ω is $U_P > 130\,eV$. This value is more than an order of magnitude below the binding energy $E_K > 3.1\,keV$ of K-shell electrons in argon. Moreover the analysis of the x-ray spectra also show that the mean charge state of the emitting ions can be as high as 13+ when irradiating argon clusters with pulses of an intensity of $I = 3 \times 10^{16}\,Wcm^{-2}$. Both these observations raise questions as to the additional heating mechanisms at play in a cluster environment, which allow the electrons to be effectively accelerated well beyond the ponderomotive energy.

Article published by EDP Sciences and available at http://www.edpsciences.org/jp4 or http://dx.doi.org/10.1051/jp4:2006138007

After a decade of experimental and theoretical studies, the mechanisms causing the efficient heating of electrons in a cluster environment are still a matter of debate [4]. In the nanoplasma model [5] fast electrons are produced by inverse bremsstrahlung. The energy absorption is greatly enhanced when the plasma frequency of the electrons in the cluster matches the laser frequency. It has, however, been argued [3, 6], that this resonance should be strongly damped and that the high energy contribution of the electronic energy distribution should not be sufficient to explain the creation of inner-shell vacancies. Molecular dynamics simulations are limited to clusters of about 1000 atoms [7-9], and a scaling of the results to larger cluster sizes is difficult. Clusters of $\sim 10^4$ atoms have been simulated using a microscopic particle in cell (MPIC) code [10]. However only predictions for the energy distribution of the emitted electrons for a laser intensity $I = 8.10^{15}$ Wcm^{-2} were made. This makes it difficult to draw conclusions as to the energy distribution of the electrons inside the cluster at lower laser intensities. Moreover, the predicted maximum ionic charge state of Ar^{6+} differs significantly from the measured mean ionic charge state of Ar^{13+} where the L-shell population is efficiently depleted.

In Section 2 we will propose elastic electron-ion scattering as an efficient electronic heating mechanism and discuss the appropriate theoretical description. In order to study the heating of the electrons quantitatively, we developed a classical trajectory Monte Carlo (CTMC) simulation describing the laser-cluster interaction, the details of which will be presented in section 3. Section 4 will contain simulation results concerning the electronic dynamics and the resulting x-ray yield, which allow quantifying the efficiency of heating by elastic electron-ion scattering.

2. ELASTIC ELECTRON-ION SCATTERING

We discuss in detail the role of elastic electron-ion scattering for the heating of quasi-free electrons in large clusters. Elastic backscattering of an electron in the core potential of an atom or ion can flip the velocity vector of the electron, and thus allows, with a non-negligible probability, to remain synchronized with the alternating laser field vector during the subsequent half-cycle. It is then possible that the electron gains additional kinetic energy instead of losing energy and momentum it has gained during the previous laser half-cycle (Fig. 1). A small sub-ensemble of electrons can thus be rapidly heated to high kinetic energies well beyond the maximum quiver energy $E_P = 2U_P$. This heating mechanism by repeated back-scattering resembles the Fermi-shuttle acceleration [11, 12] and is also related to the lucky-electron model proposed for IR photoemission from metallic surfaces [13].

The efficiency of this heating mechanism depends critically on the accurate theoretical description of the elastic scattering process. The scattering into backward angles ($\theta\tau 90^\circ$), which is of particular importance for this mechanism, is determined by the short-ranged non-Coulombic contributions to the ionic core potential. As these contributions are neglected in frequently used descriptions of ions in terms of softened Coulomb potentials, the effect of backscattering is left unaccounted for in many simulations [8-10]. In the present work we calculate the differential scattering cross-sections for the electrons $d\sigma_e/d\theta$ by partial wave analysis of parametrized Hartree-Fock potentials [14, 15]. The differential cross-section is typically dominated by few low order partial waves giving rise to generalized Ramsauer-Townsend minima [16] and diffraction oscillations [17] (Fig. 2). To account for solid-state effects a muffin-tin potential is employed in the interstitial region [15], which, however, has effectively little influence on the scattering into large angles. For moderate electron energies (δkeV), the cross-section for backward angles exceeds the Rutherford cross-section (pure Coulomb case) by several orders of magnitude for all charge states (Fig. 2).

3. NUMERICAL MODEL

Due to the large size of the clusters (N > 10000 atoms), a full ab-initio simulation seems still impractical. We therefore opt for a simplified theoretical description of the dynamics of the laser-cluster interaction [18].

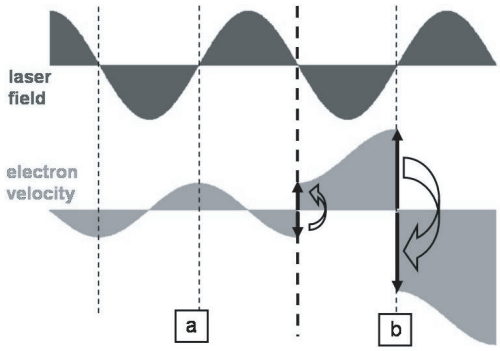

Figure 1. Time evolution of the velocity of an electron in a laser field, schematically. A free electron loses its previously gained momentum in each half-cycle of the laser (a). If the velocity of the electrons is flipped, a subensemble of electrons can efficiently gain kinetic energy in the laser field.

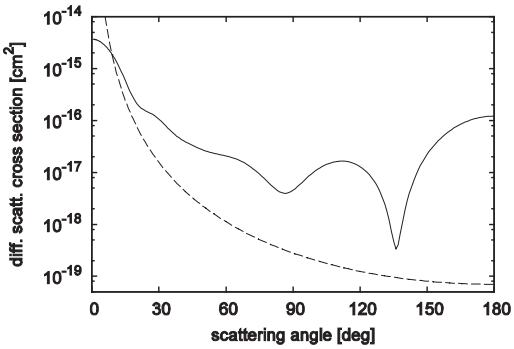

Figure 2. Differential cross-section $d\sigma_e/d\theta$ for elastic scattering of an electron with kinetic energy E = 10 a.u. at Ar^{2+} (solid line). The Rutherford cross-section is also displayed (dashed line).

3.1 Ionic dynamics

Because of their large inertia, the dynamics of the cluster ions proceeds on the time scale of the laser pulse. We therefore describe the ions of mass M and mean charge state ⟨q(t)⟩ as a uniform spherical positive background charge with a time dependent radius R(t). As some quasi-free electrons leave the cluster (outer ionization), the cluster of radius R(t) is charged and acquires the positive cluster charge Q(R,t). The monopole field resulting from this charging drives the cluster expansion. For a realistic estimate of the time evolution of the cluster radius R(t), we take into account that the ionic charge ⟨q(t)⟩ is screened by the surrounding quasi-free electrons. We determine R(t) from the equation of motion of an ion with the screened charge state $\langle q_{scr}(t)\rangle$, situated at the surface of the cluster (r = R(t)):

$$M\frac{d^2R(t)}{dt^2} = \frac{\langle q_{\mathrm{scr}}(t)\rangle \cdot Q(R,t)}{R(t)^2}. \tag{1}$$

To estimate the screened charge state $\langle q_{scr}(t)\rangle$ of the ions on the cluster surface, we reduce ⟨q(t)⟩ corresponding to the number of quasi-free electrons per ion:

$$\langle q_{\mathrm{scr}}(t)\rangle = \langle q(t)\rangle - n_e(R,t)/\rho(t), \tag{2}$$

where $(-n_e(R,t))$ is the local electronic charge density on the surface of the cluster and $\rho(t)$ is the ionic number density.

3.2 Electronic dynamics

To describe the electronic dynamics, we employ a test-particle discretization, i.e. we solve the equations of motion only for a representative fraction of the ensemble of particles. The representation fraction α is limited by computational capabilities.

The test-particle ensemble of the $i = 1, \ldots, N_{test}(t) = \alpha N_e(t)$ electrons obeys the following Langevin equation:

$$\ddot{\vec{r}}_i = -\vec{F}_L(t) - \vec{F}_{\mathrm{mean}}(\vec{r}_i, t) + \vec{F}_{\mathrm{stoc}}(\vec{r}_i, \dot{\vec{r}}_i, t). \tag{3}$$

This approach can also be seen as a generalization of classical transport theory (CTT) [19] for a dynamical system open to both particle number variation $N_{test}(t)$ and energy exchange with the

many-particle reservoir (ions and electrons), as well as with the laser field. As the cluster is much smaller than the wavelength of the laser pulse ($R(0) \ll \lambda$), the laser can be described as a uniform time-dependent electric field with a Gaussian amplitude envelope, which is linearly polarized in the z-direction:

$$\vec{F}_L(t) = F_0 \hat{z} \sin(\omega t) \exp\left(-2 \ln 2 \frac{(t-2\tau)^2}{\tau^2}\right). \tag{4}$$

Electron-electron and electron-ion interactions are taken into account by the time-dependent mean field $\vec{F}_{\text{mean}}(\vec{r}, t)$, which depends on the positions of all test particles. The mean field is approximated by the monopole and dipole contributions to its multipole expansion. The monopole term is given by:

$$\vec{F}^{(0)}_{\text{mean}}(\vec{r}, t) = Q(r, t) \frac{\vec{r}}{r^3}, \tag{5}$$

where Q(r,t) stands for the instantaneous charge contained in the sphere of radius r resulting from the possible imbalance between the number of electrons and the ionic background charge. Q(r,t) is evaluated by discretizing a sphere of radius 2R(t) including the cluster of radius R(t) and the surrounding simulation volume up to 2R(t) in 20 concentric spherical shells of equal distance. The dipole contribution to the mean field arises from the laser induced shift of the electron sphere with respect to the ion sphere. The dipole field can therefore be estimated as the field of a polarized sphere:

$$\vec{F}^{(1)}_{\text{mean}}(\vec{r}, t) = -\frac{\vec{p}(t)}{R(t)^3}, \tag{6}$$

where the dipole moment $\vec{p}(t)$ is determined by the position of all the test particles within the sphere:

$$\vec{p}(t) \cong -\frac{1}{\alpha} \sum_{r_i < R(t)} \vec{r}_i. \tag{7}$$

Momentum changes due to collision processes are taken into account by the stochastic forces $\vec{F}_{\text{stoc}}(\vec{r}_i, \dot{\vec{r}}_i, t)$. For example, elastic electron-ion scattering is determined by the probability of each electron to scatter elastically during the time step Δt:

$$P_e = \sigma_e(\langle q \rangle, E) \rho(t) \dot{\vec{r}}_i \Delta t, \tag{8}$$

which is determined by the energy (E) and charge state (q) dependent total elastic scattering cross-section σ_e, the ionic density $\rho(t)$ and the velocity of the electron. If the electron scatters, the scattering angle θ is determined randomly according to the differential cross-section $d\sigma_e/d\theta$. The change in momentum associated with this scattering of angle θ is one contribution to the stochastic force $\vec{F}_{\text{stoc}}(\vec{r}_i, \dot{\vec{r}}_i, t)$. Further contributions are, for example, electron-impact ionization of the outer-shell electrons and K-shell ionization. These events are not only marked by a change in momentum, but also by a change in the number of test particles $N_{\text{test}}(t)$, as well as in the mean number of bound electrons in the respective shells $N_M(t)$, $N_L(t)$ and $N_K(t)$.

3.3 Ionization mechanisms

The binding energies E_L and E_M of electrons in the L-shell and M-shell of an argon ion are estimated by the following empirical formulas (in atomic units):

$$E_M(N_L, N_M) = 12.47 - 0.89 N_L - 0.62 N_M \tag{9a}$$

$$E_L(N_L, N_M) = 33.3 - 2.25 N_L - 0.79 N_M \tag{9b}$$

where N_L and N_M stand for the number of electrons in the L-shell and M-shell. These formulas are approximations for argon ions with 2 electrons in the K-shell and are based on spectroscopic data

of binding energies [20, 21]. The binding energy E_K of the K-shell electrons is assumed to be only dependent on the charge state q of the ion [20]:

$$E_K(q) = 117.8 + 1.3q \quad \text{for q} \leq 8$$

$$E_K(q) = 108.6 + 2.4q \quad \text{for } 8 < \text{q} \leq 16. \tag{10}$$

Field ionization takes place when the combined field of the laser field and dipole field inside the cluster exceeds the threshold field F_{OBI} for over-barrier ionization

$$F_{\text{OBI}} = \frac{W(N_L, N_M)^2}{4(q+1)}, \tag{11}$$

which is determined by the ionization potential W of an argon ion with charge q, 2 electrons in the K-shell, N_L electrons in the L-shell and N_M electrons in the M-shell. In the event of field ionization, all ions are ionized once, i.e. αN new test particles with zero velocity are distributed uniformly in the cluster.

Additional quasi-free electrons can be created by electron-impact ionization which is treated as stochastic process. The cross-section for impact ionization by an electron with kinetic energy E is evaluated from the Lotz formula [22] (the step functions Θ(x) assure that the corresponding energy thresholds are exceeded):

$$\sigma_{\text{ei}} = 2.17 \left(N_M \frac{\ln(E/E_M)}{E \cdot E_M} \Theta(E - E_M) + N_L \frac{\ln(E/E_L)}{E \cdot E_L} \Theta(E - E_L) \right). \tag{12}$$

Furthermore the contribution of two-step ionization (electron-impact excitation from L-shell to M-shell followed by an impact ionization) is roughly estimated by assuming the cross-section for impact excitation to be:

$$\sigma_{\text{L}\to\text{M}} = 2.17 N_L \frac{\ln(E/(E_L - E_M))}{E \cdot (E_L - E_M)} \Theta(E - E_L - E_M). \tag{13}$$

The Auger decay of the L-shell vacancies is incorporated in the simulation by creating new test particles with the rate $1/\tau_{\text{A}} \approx 5.7 \times 10^{-3}$a.u. [23].

It has been proposed [24] that, in the case of a cluster ion, ionization may be enhanced by the proximity of the surrounding highly charged ions. The additional Coulomb potential of its neighbour lowers the Coulomb barrier of the ion. We estimate the lowering of the ionization threshold due to the superposition of the two Coulomb potentials to be:

$$\Delta W = -2 \frac{\langle q_{scr}(t) \rangle}{d_{ii}/2}, \tag{14}$$

where $d_{ii} = \rho^{-1/3}$ is the mean ion-ion distance.

4. SIMULATION RESULTS

Figures 3-6 present typical simulation results obtained when solving Eq. (3) for a cluster with $\text{N} = 2.8 \times 10^5$ argon atoms irradiated by an infrared ($\lambda = 800\,\text{nm}$) laser pulse of pulse duration $\tau = 60$fs with a peak intensity of $\text{I} = 1.6 \times 10^{16}\,\text{Wcm}^{-2}$. The cluster has initially a solid density of $\rho(\text{t} = 0) = 2.66 \times 10^{22}\,\text{cm}^{-3}$ and the initial cluster radius is R(0) = 258 a.u.. The first $N_{\text{test}}(t_1)$ test particles are released with zero velocity and random positions in the cluster as soon as the laser field reaches the threshold for the over barrier ionization of the neutral argon atoms ($F_{\text{OBI}} > 0.08$ a.u.). These particles provide the initial conditions for the propagation of Eq. (3). In the present case the representation fraction is chosen to be $\alpha = 0.05$. The number of test particles increases rapidly (Fig. 4) due to the

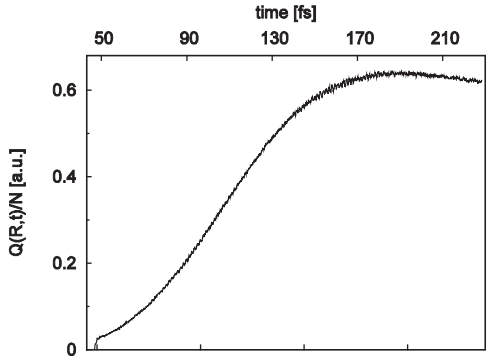

Figure 3. Time evolution of the total cluster charge per atom.

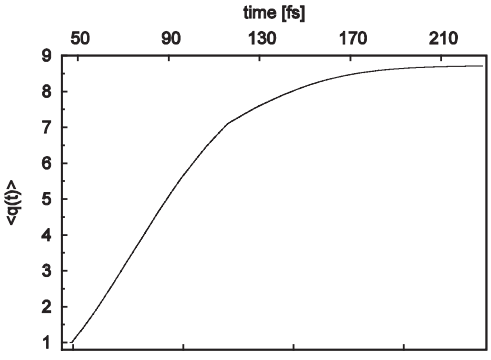

Figure 4. Time evolution of the mean ionic charge state.

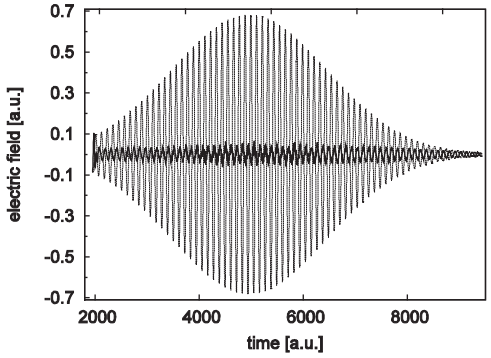

Figure 5. Time evolution of the laser field (dashed) and the effective field (solid).

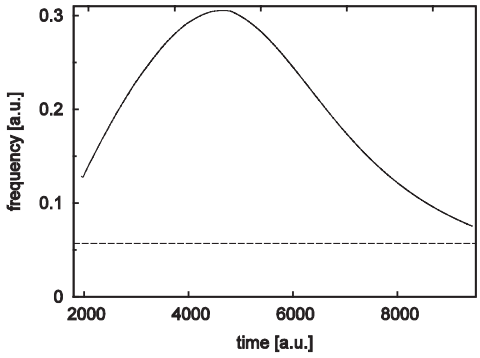

Figure 6. Time evolution of the laser frequency (dashed) and the plasma frequency (solid).

efficient ionization of the cluster. The secondary ionization mechanisms discussed in the previous section (excitation, Auger decay and ion proximity) form only a minor contribution to the ionization process, which is dominated by electron impact ionization of the outermost atomic shell. By the end of the laser pulse, a mean ionic charge state of Ar^{9+} is reached. Even though this is significantly higher than the maximum charge state of Ar^{6+} found in Ref. [10], the efficient depletion of the L-shell associated with the mean charge state of Ar^{13+} found experimentally [3] can not yet be fully explained. The total cluster charge resulting from electrons leaving the cluster (Fig. 3) results in an expansion of the cluster radius by less than a factor 3 during the laser pulse. Furthermore the simulations show that the charge is concentrated on the cluster surface, the interior of the cluster being well shielded by the quasi-free electrons. Inside the cluster the effective field acting on the electrons is therefore the sum of the laser field and the dipole field:

$$\vec{F}_{\text{eff}}(t) = \vec{F}_L(t) + \vec{F}^{(1)}_{\text{mean}}(t).$$

Due to the polarization of the cluster, the effective field inside the cluster is strongly reduced compared to the laser field (Fig. 5). This can also be understood in terms of the plasma frequency ω_{P}. After the first ionization event ($t = t_1$), the plasma frequency is $\omega^2_{\text{P}}(t_1) = N_{\text{test}}(t_1)/(\alpha R(t_1)^3) \approx 5\omega^2$. Due to the efficient ionization, ω_{P} first increases rapidly, before diminishing in the second half of the pulse

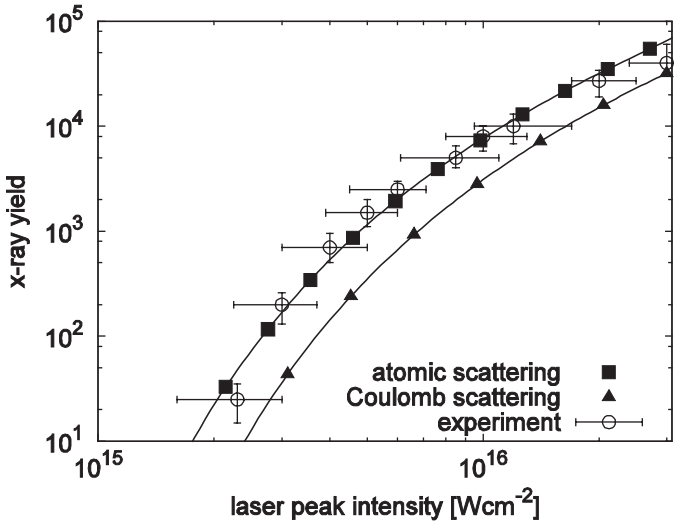

Figure 7. Absolute x-ray yield as a function of the laser peak intensity. Experimental results (○), simulation results obtained with a Coulomb potential for the description of the ions (▲) and obtained with the realistic ionic potential (see text) (■).

as the cluster begins to expand (Fig. 6). Following Ref. [5], the mean field can be estimated as

$$\vec{F}_{\text{eff}}(t) \approx Re\left\{\int_{\omega-\Delta\omega}^{\omega+\Delta\omega} \tilde{\vec{F}}_L(\omega')\left(1-\frac{\omega_P^2}{\omega_P^2-\omega'^2-i\omega'\gamma}\right)e^{i\omega' t}d\omega'\right\}, \tag{15}$$

where $\Delta\omega$ is the Fourier width associated with the temporal profile of the pulse (4) and γ stands for the damping constant due to scattering events. As the plasma frequency exceeds the laser frequency ω during the whole duration of the laser pulse (Fig. 6), the effective field is smaller than the laser field. It is worth noting that no plasma resonance $\omega_{\text{P}} = \omega$ occurs in this range of parameters.

The x-ray yield per cluster is determined by the number of K-shell vacancies created, corrected by the mean fluorescence yield $\eta = 0.12$ [23]. Furthermore, the spatial Gaussian intensity profile of the laser beam [3] has to be taken into account to obtain the absolute x-ray yield. The simulation results are compared to the experimental results in Fig. 7. In order to estimate the efficiency of heating by elastic electron-ion scattering, the simulation carried out with the parametrized Hartree-Fock potential describing the ionic potential is compared to an otherwise identical simulation where a pure Coulomb potential describes the elastic electron-ion interaction. In both cases for $\text{I} > 2 \times 10^{15}\,\text{Wcm}^{-2}$ a small fraction of electrons gains sufficient energy to produce K-shell vacancies. This can be associated with the heating in the monopole field of the charged-up cluster. However including the realistic scattering potential and thereby allowing for elastic backscattering events, drastically increases the x-ray yield by a factor 3-5 compared to the pure Coulomb case. This effect is the most pronounced at low intensities, i.e. close to the threshold. As the laser intensity increases, the cross-section for backscattering decreases due to the higher energy of the electrons. The simulation results in Fig. 7 were scaled down by a factor 2 to fit the experimental results. This factor is well within the experimental uncertainty associated with the number of clusters in the interaction volume.

In summary we have identified elastic electron-ion large-angle scattering as a heating mechanism efficient for moderate laser intensities ($\text{I} = 1 \times 10^{15} - 3 \times 10^{16}\,\text{Wcm}^{-2}$) and large clusters ($\text{N} > 10^4$ atoms). Our simulation which is based on a mean-field approach gives x-ray yields in surprisingly good agreement with the experimental results.

This work is supported by FWF SFB-16 (Austria).

References

[1] V.P. Krainov and M.B. Smirnov, Phys. Rep. **370**, 237 (2002).
[2] E. Lamour, C. Prigent, J.P. Rozet and D. Vernhet, Nucl. Instr. and Meth. Phys. Res. B **235**, 408 (2005).
[3] C. Prigent, Ph.D. thesis, Université Pierre et Marie Curie, Paris VI, 2004.
[4] U. Saalmann, Ch. Siedschlag and J.M. Rost, J. Phys. B **39** R39 (2006).
[5] Ditmire T., Donnelly T. and Rubenchik A.M. et al., Phys. Rev. A **53**, 3379-3402 (1996).
[6] F. Megi, M. Belkacem, M.A. Bouchene, E. Suraud and G. Zwicknagel, J. Phys. B **36**, 273 (2003).
[7] C. Rose Petruck, K.J. Schafer and K.R. Wilson et al., Phys. Rev. A **55** (1997) 1182-1190.
[8] I. Last and J. Jortner, Phys. Rev. A **60**, 2215 (1999).
[9] U. Saalmann and J.M. Rost, Phys. Rev. Lett. **91**, 233401.
[10] C. Jungreuthmayer, M. Geissler, J. Zanghellini and T. Brabec, Phys. Rev. Lett. **92**, 133401 (2004).
[11] E. Fermi, Phys. Rev. **75**, 1169 (1949).
[12] J. Burgdörfer, J. Wang and R.H. Ritchie, Phys. Scr. **44**, 391 (1991).
[13] F. Pisani et al., Phys. Rev. Lett. **87**, 187403 (2001).
[14] P.P. Szydlik and A.E.S. Green, Phys. Rev. A **9**, 1885 (1974).
[15] F. Salvat and R. Mayol, Comp. Phys. Comm. **74**, 358 (1993).
[16] N. Mott and H. Massey, *Theory of Atomic Collisions*, Oxford University Press, New York, 1965.
[17] J. Burgdörfer, C.O. Reinhold, J. Sternberg and J. Wang, Phys. Rev. A **51**, 1248 (1995).
[18] C. Deiss et al., Phys. Rev. Lett. **96**, 013203 (2006).
[19] J. Burgdörfer and J. Gibbons, Phys. Rev. A **42**, 1206 (1990).
[20] W. Lotz, J. Opt. Soc. Am. **58**, 915 (1968).
[21] Y. Ralchenko et al., *NIST Atomic Spectra Database* (version 3.0.3), http://physics.nist.gov/asd3 (2005).
[22] W. Lotz, Z. Phys. **216**, 241 (1968).
[23] C.P. Bhalla, Phys. Rev. A **8**, 2877 (1973).
[24] Ch Siedschlag and J.M. Rost, Phys. Rev. A **67**, 013404 (2003).